BAF chromatin complexes do not mediate GLI transcriptional repression of Hedgehog target genes

Janani Ramachandran[1], Wanlu Chen[2], Rachel K. Lex[1], Kathryn E. Windsor[1], Hyunji Lee[1], Tingchang Wang[2], Weiqiang Zhou[2], Hongkai Ji[2] and Steven A. Vokes[1*]

[1]Department of Molecular Biosciences, University of Texas at Austin, 100 E 24th Street Stop A5000, Austin, TX 78712 USA

[2]Department of Biostatistics, Johns Hopkins Bloomberg School of Public Health, 615 North Wolfe Street, Baltimore, MD 21205, USA

[*]Corresponding author

Email: svokes@austin.utexas.edu

Phone: +1 512-232-8359

Keywords: Hedgehog, GLI3, transcriptional repression, limb bud, BAF, SWI/SNF

ABSTRACT

The Hedgehog (HH) signaling pathway is primarily modulated by GLI transcriptional repression in the mouse limb. Previous studies have suggested a role for the BAF chromatin remodeling complex in mediating GLI repression. Consistent with this possibility, the core BAF complex protein SMARCC1 is present at most active limb enhancers including the majority of GLI enhancers. Despite this, we find that SMARCC1 maintains chromatin accessibility at GLI enhancers suggesting that it contributes to enhancer activation rather than helping to mediate GLI repression. Furthermore, SMARCC1 binds GLI-regulated enhancers independently of GLI3 and does not facilitate transcriptional repression of most GLI target genes. Finally, *Smarcc1- and Shh*- double knockout phenotypes suggest that SMARCC1 is not required to mediate constitutive GLI repression in HH mutants. We conclude that the BAF complex does not mediate GLI3 repression, which we propose instead utilizes alternative chromatin remodeling complexes.

INTRODUCTION

The Hedgehog (HH) pathway is a multifaceted regulator of embryonic development with distinct roles in regulating the formation of most organs. Diverse cell types respond to HH signaling through cell-specific transcriptional responses mediated by GLI transcription factors. GLI proteins are bifunctional, acting as context-dependent transcriptional activators (when HH signaling is active) or transcriptional repressors (in the absence of HH). GLI repressors are particularly important in the limb bud where most HH target genes are activated solely by a loss of GLI repressor (GLI de-repression) (Lewandowski et al., 2015; Litingtung et al., 2002; teWelscher et al., 2002). Constitutive GLI repression causes reductions in H3K27 acetylation (H3K27ac), a marker associated with active enhancers, as well as reductions in ATAC-seq accessibility (Creyghton et al., 2010; Heintzman et al., 2009; Lex et al., 2020; Rada-Iglesias et al., 2011). This suggests that GLI represses transcription by inactivating enhancers through

interactions with an HDAC-containing repression complex. Additional unknown factors likely contribute to regulating chromatin accessibility as well as enhancer specificity (Lex et al., 2020). Several co-factors or complexes have been proposed to regulate GLI transcription based on physical and genetic association (Chen et al., 2004; Dai et al., 2002; Huang et al., 2016; Zhang et al., 2013; Zhang et al., 2013). However, it has been challenging to specifically link them to GLI regulation through standard genetic analysis since most co-factors are inherently pleiotropic, affecting the transcriptional regulation of multiple signaling pathways.

The SWI/SNF BAF complex has emerged as a top candidate for mediating both GLI activation and repression. This is based on evidence identifying physical interactions between multiple GLI proteins and several BAF complex members, mutations in various BAF components that alter expression of HH target genes, and that several BAF components bind to the promoters of HH target genes *Gli1* and *Ptch1* (Jagani et al., 2010; Jeon and Seong, 2016; Shi et al., 2014; Shi et al., 2016; Xiong et al., 2013; Zhan et al., 2011). BAF complexes are large, variable complexes that contain either SMARCA2 or SMARCA4, proteins with ATPase domains that mediate changes in nucleosomal density at enhancers or promoters. BAF complexes also include several core components, including SMARCC1 which promotes ATPase activity as well as the stability of BAF proteins (Clapier et al., 2017; Sohn et al., 2007; Sokpor et al., 2017).

Since BAF complexes broadly maintain enhancer accessibility and H3K27ac enrichment across many different pathways, it is unclear how they might mechanistically mediate GLI repression (Alver et al., 2017; Hendy et al., 2022; Wang et al., 2017). As GLI transcriptional repression promotes reduced enhancer accessibility and H3K27ac enrichment, it would seem more likely that these changes would be facilitated by loss of BAF complex activity rather than its presence. Additionally, the relatively global requirements for BAF complexes at many developmental enhancers indicate that they have upstream roles in regulating enhancer accessibility that might

be distinct from GLI3 repression. Nonetheless, BAF complexes bind to GLI3 repressor isoforms and a loss of BAF activity results in the expansion of some GLI target genes (Jagani et al., 2010; Jeon and Seong, 2016; Zhan et al., 2011). Moreover, it has been reported that the BAF component SMARCA4 mediates both GLI activation and repression (Zhan et al., 2011). These studies, which have examined a few signature target genes of the HH pathway are consistent with the notion that BAF complex could mediate GLI repression. In keeping with this possibility, BAF complexes can repress transcription in certain cases where they reposition a repressive nucleosome (Rafati et al., 2011). Additional scenarios in which GLI3 repressor complexes bind to and attenuate BAF complex activity are also possible.

To clarify the role of BAF complexes in HH gene regulation, we tested the hypothesis that a BAF complex mediates GLI repression in the limb by conditionally knocking out the core component *Smarcc1* in limb buds and examining the genomic response at GLI enhancers and target genes. Consistent with previous studies, the loss of *Smarcc1* results in a loss of accessibility at thousands of genomic regions and disrupts the expression of several specific HH target genes. However, the expression of most HH target genes is not affected by loss of *Smarcc1*, and GLI3 does not recruit or maintain SMARCC1 at most GLI enhancers. Moreover, loss of *Smarcc1* is not sufficient to ameliorate the digit phenotypes caused by constitutive GLI repression in $Shh^{-/-}$ limb buds, supporting the fact that SMARCC1 does not mediate global GLI repression. We conclude that the BAF complex does not act as a co-factor for GLI repression.

RESULTS AND DISCUSSION

SMARCC1 binds to most active limb enhancers and the majority of GLI-binding regions

To determine if BAF complexes are present at GLI enhancers in the mouse limb bud, we identified the genomic binding regions for SMARCC1, a core component of BAF complexes that serves a scaffolding role and protects other members of the complex from proteolytic degradation (Chen and Archer, 2005; Sohn et al., 2007). We dissected limb buds into anterior and posterior halves and identified a combined total of 48,268 SMARCC1-bound regions at E11.5 using CUT&RUN (Figure 1A). The majority of SMARCC1-bound regions (22,344) were common to both the anterior and posterior limb buds, and most (~69%) were enriched for the active enhancer mark H3K27ac consistent with prior reports of BAF complex recruitment to H3K27ac-enriched active enhancers (Figure 1A-B; Source data 1) (Creyghton et al., 2010; Heintzman et al., 2009; Malkmus et al., 2021; Rada-Iglesias et al., 2011). To understand the extent to which SMARCC1 broadly regulates enhancers, we assessed SMARCC1 binding at H3K27ac ChIP-seq peaks as well as validated enhancers from the VISTA Enhancer Browser (Visel et al., 2007). Consistent with a global role for BAF in regulating active enhancers, approximately half of all H3K27ac-enriched regions (52%), and most (87%) of the annotated VISTA limb enhancers were bound by SMARCC1 (Figure 1B, Supp. Figure 1A-C), (Alver et al., 2017; Park et al., 2021). In addition to regions that were bound by SMARCC1 in both anterior and posterior limb bud halves, there were a smaller portion of anterior-specific (5,738) and posterior-specific (20,186) regions (Figure 1A). These included VISTA limb enhancers with enhancer activity in the same anterior/posterior region, suggesting that they correspond to spatially restricted limb enhancers (Figure 1C, Supp Figure 1A-C).

To determine if BAF complexes are associated with GLI repressor-bound regions, we intersected SMARCC1 binding regions in anterior halves (where there are high levels of GLI repression) with a set of previously identified regions that are primarily or exclusively bound by GLI3-repressor (Lex et al., 2022). Most GLI3 binding regions (~80%) were also bound by SMARCC1 in the anterior limb (Figure 1D-E), including the subset of HH responsive GLI binding

regions (hereafter referred to as 'GLI-enhancers') that are enriched around HH target genes (Supp Figure 1D) (Lex et al., 2020). We conclude that SMARCC1 binds to a large number of active enhancers in the limb, including regions bound by GLI3. We next sought to determine if SMARCC1 is required for regulating chromatin accessibility in response to GLI repression.

SMARCC1 maintains chromatin accessibility throughout the genome including GLI enhancers

Since GLI repression is associated with a reduction in chromatin accessibility (Lex et al., 2020; Lex et al., 2022), we sought to determine if BAF complexes mediate this aspect of GLI repression by conditionally deleting *Smarcc1* in limb buds. Consistent with previous studies, SMARCA4 levels were reduced in $Prx^{Cre/+};Smarcc1^{c/c}$ (here after referred to as 'SMARCC1 cKOs') limb buds (Supp. Figure 2A) (Jeon and Seong, 2016). We then identified ATAC-accessible regions in the anterior halves of limb buds from E11.5 control and SMARCC1 cKOs (Figure 2A). More than 10% of all ATAC-accessible regions (10,906/100,188) had significantly reduced accessibility in SMARCC1 cKO limb buds (FDR<0.05), 58% (6,279/10,906) of which were enriched for H3K27ac (Figure 2B-D, E, Source data 3). Approximately 50% (154/309) of GLI enhancers also showed significantly reduced accessibility (Figure 2B-D, E, Source data 3), suggesting that *Smarcc1* is required to maintain open chromatin throughout the genome, including the majority of HH-responsive enhancers. Thus, rather than mediating GLI3-regulated chromatin compaction, SMARCC1 has a major genomic role in maintaining enhancer accessibility.

GLI3 and SMARCC1 are independently recruited to nascent and active GLI enhancers

We asked if GLI3 might recruit SMARCC1 to nascent GLI enhancers by examining SMARCC1-binding in early limb buds prior to the apparent onset of GLI repression (Lex et al., 2022). At this stage, 60% (128/216; Source data 1) of the GLI enhancers that bound by GLI3 in early limb buds were not bound by SMARCC1. Conversely, most GLI enhancers bound by SMARCC1 at E9.25 also had GLI3 enrichment at this stage (88/104), were enriched for H3K27ac (70/104), and positioned intragenically or proximal to gene promoters (82/104) (Figure 3A). These included *Gli1,* a HH-target gene that is primarily regulated by a promoter-proximal enhancer, and *Cdk6* (Figure 3 A-C) (Lopez-Rios et al., 2012; Vokes et al., 2008). This indicates that GLI3 binds most nascent GLI enhancers without SMARCC1 and that BAF complexes become associated with most GLI enhancers only at later stages (Fig. 1D-E; Supp. Figure 1D). This is in contrast to previous reports that have shown BAF recruitment to poised early enhancers in human embryonic stem cells (Rada-Iglesias et al 2011) and suggests tissue-specific recruitment of BAF complexes to early enhancers. We conclude that GLI3 alone is not sufficient to recruit BAF complexes to nascent limb enhancers.

To determine if GLI3 maintains SMARCC1 after the onset of HH signaling, we examined differential SMARCC1 binding in sibling control (*Gli3*$^{+/+}$) and *Gli3*$^{-/-}$ anterior halves of forelimbs at E11.5, when SMARCC1 and GLI3 binding co-occur (Figure 3D). SMARCC1 was bound to 79% of GLI enhancers (245/309) in control limbs, and the majority of these regions (188/245) remained bound by SMARCC1 in *Gli3*$^{-/-}$ limbs (Figure 3E, Source data 4). This indicates that SMARCC1 is bound to most GLI enhancers even in the absence of *Gli3* and includes biologically validated HH targets such as *Ptch1*, *Gli1* and *Cdk6* (Figure 3E, G-H). SMARCC1 was recruited to most GLI-bound enhancers (188/194 total regions) in *Gli3*$^{-/-}$s. The 57 regions that appeared to lose SMARCC1 in *Gli3*$^{-/-}$s generally had some detectable SMARCC1 binding in 1 or more mutant replicates, suggesting that variability among *Gli3*$^{-/-}$ embryos may have contributed to a loss in the number of significantly called SMARCC1 peaks (Figure 3E, Supp.

Figure 3). Although SMARCC1 remained bound to most GLI enhancers in the absence of GLI3, there was a small but significant reduction in the overall enrichment levels of SMARCC1 in *Gli3*$^{-/-}$ limbs compared to controls for reasons that are presently unknown (Figure 3F, Source data 4). Overall, SMARCC1 is retained at the majority of GLI enhancers in the absence *Gli3*, suggesting that GLI3 likely does not recruit or maintain SMARCC1 at enhancers, but instead that SMARCC1 binds and regulates chromatin accessibility at enhancers in a GLI3-independent fashion. These results do not exclude a secondary role for a specific type of BAF complex in mediating later GLI-specific chromatin compaction after enhancer activation and given previous reports of *Smarcc1*-dependent de-repression of some HH-target genes in the limb (Jeon and Seong, 2016), we sought to determine if SMARCC1 is required for the transcription of HH target genes.

Smarcc1 **is not required for most HH target gene expression**

To determine the role of BAF in mediating GLI transcriptional repression, we compared gene expression between wild-type controls and SMARCC1 cKOs in E11.5 limb buds. The 928 differentially expressed genes included approximately one-third (19/63) of previously predicted GLI target genes including *Gli1* and *Hhip* (Lex et al., 2022) (Figure 4A and Supp. Figure 4B; Source data 5). Notably, several biologically validated and well established HH target genes, including *Ptch1*, *Hand2* and *Cdk6* were not significantly changed (Figure 4A; Supp. Figure 4B). In addition, most GLI3-responsive genes previously shown to be upregulated in *Gli3*$^{-/-}$ limb buds (125/146) were not significantly upregulated in the absence of *Smarcc1* (Figure 4B) (Lex et al., 2022). This suggests that the majority of GLI-repressor target genes are not SMARCC1-dependent. A caveat to this interpretation is that the *Hand2* expression domain has previously been shown to be anteriorly expanded in *Prx*$^{Cre/+}$*;Smarcc1*$^{c/c}$ limb buds, indicating limitations to the sensitivity of the RNA-seq performed on whole limb buds (Jeon and Seong, 2016).

Additional pathway analysis of *Smarcc1*-responsive genes indicated enrichment of the WNT, Hippo, BMP and FGF signaling pathways as well as limb-specific transcription factors (i.e. *Tbx3*, *Tbx4*, and *Alx4*) (Supp. Figure 4A-B). Overall, this suggests that SMARCC1 regulates gene expression underlying many limb pathways but does not have a specific role in GLI transcriptional regulation. This is further supported by differences in the polydactylous phenotype observed in SMARCC1 cKOs compared to $Gli3^{-/-}$ limb buds. Consistent with prior reports, SMARCC1 cKOs have variable numbers of forelimb digits ranging from oligodactyly to polydactyly with polydactyly in the hindlimbs (n=3; Supp. Figure 4C-F) (Jeon and Seong, 2016). In contrast, $Gli3^{-/-}$ forelimbs have uniform forelimb polydactyly and lack the distinct distal digit fusions present in SMARCC1 cKOs mutants, suggesting that the digit phenotypes observed in SMARCC1 cKOs are likely not due to GLI de-repression alone (Bowers et al., 2012; Mo et al., 1997).

SMARCC1 is not required for GLI3 repression

The above experiments suggest that SMARCC1 does not uniformly mediate global GLI repression. However, some HH target genes require SMARCC1 for normal expression, suggesting that BAF complexes might co-regulate a subset of GLI targets that are critical for limb development. *Shh;Gli3* double mutants greatly improve the digit and limb phenotypes seen in $Shh^{-/-}$ embryos, indicating that loss of GLI3 repression is sufficient to rescue many aspects of the $Shh^{-/-}$ phenotype (Chiang et al., 2001; Lewandowski et al., 2015; Litingtung et al., 2002; teWelscher et al., 2002). If SMARCC1 is required for GLI3 repression, then the loss of *Smarcc1* should result in a partial rescue of digit number and limb size in $Shh^{-/-}$ limb buds. To test this, we compared the phenotypes in $Shh^{-/-}$ and $Prx^{Cre/+};Smarcc1^{c/c}$ (hereafter referred to as 'DKO') limb buds at E12.5, a stage when digit specification has already occurred. Wild-type embryos had 5 distinct *Sox9*-expressing digit condensates on both their forelimbs and hindlimbs (n=3)

while *Prx*$^{Cre/+}$*; Smarcc1*$^{c/c}$ limb buds had variable numbers of abnormally patterned condensates (n=4). In contrast, loss of *Smarcc1* was unable to rescue the *Shh* phenotype: DKO forelimbs and hindlimbs were indistinguishable from *Shh*$^{-/-}$ (n=4 of each genotype; Figure 4C-J). A limitation to interpreting these results is that GLI3 repression and HH signaling have essential early roles in limb specification and thus it is possible that *Smarcc1* conditional deletion occurs too late to rescue the phenotype (Lex et al., 2022; Scherz et al., 2007; Zhu et al., 2008; Zhu et al., 2022). However, the conditional deletion of *Shh* results in a hypomorphic phenotype with reduced numbers of digits, suggesting that inhibition of GLI repression should have resulted in some improvement of the phenotype. In addition, the onset of *PrxCre* occurs earlier in the hindlimb than in the forelimb yet there was no improvement in the DKO hindlimbs either (Logan et al., 2002). Finally, SMARCC1 does not bind to the majority of GLI3-bound HH-responsive enhancers at early stages (Figure 3A, C) suggesting that it likely has a very limited role, if any, in GLI enhancer regulation prior to HH-signaling onset.

We have shown that *Smarcc1* does not repress the transcription of the majority of HH-target genes, suggesting that previously reported *Smarcc1*-related limb phenotypes might be caused by general disruption of limb patterning and growth rather than the uniform disruption of GLI repression. Our finding that SMARCC1 is not necessary for GLI repression in the absence of HH signaling contrasts with previously reported findings in cultured mouse embryonic fibroblasts indicating that BAF complexes are required for GLI repression (Zhan et al., 2011). This conclusion was primarily drawn from observations of the HH target genes *Ptch1* and *Gli1*, which had increased expression in the absence of the BAF component SMARCA4. However, both of these genes have a specific requirement for GLI activation, suggesting that the increase in transcription in the absence of BAF activity does not reflect a role in GLI de-repression (Litingtung et al., 2002; teWelscher et al., 2002). In the absence of a specific role in GLI repression, we propose that BAF complexes are independently enriched at most active

enhancers, including GLI enhancers where they regulate chromatin accessibility. This is distinct from parallel GLI transcriptional repression that recruits still unknown chromatin complexes (Figure 4J-K). Thus, despite demonstrated binding to BAF complex members, including SMARCC1, GLI3 repressor functions independently of SMARCC1 at GLI enhancers.

METHODS

Mouse strains and limb tissue isolation

Experiments involving mice were approved by the Institutional Animal Care and Use Committee at the University of Texas at Austin (protocol AUP-2022-00221). The *Smarcc1*$^{tm2.1Rhs}$ conditional allele (Jeon and Seong, 2016) (referred to as *Smarcc1*$^{c/+}$) was maintained on a C57/BL6 background and crossed with *Prx1*$^{Cre/+}$ mice (Logan et al., 2002) to generate control (*Prx*$^{Cre/+}$*;Smarcc1*$^{c/+}$) and *Prx*$^{Cre/+}$*;Smarcc1*$^{c/c}$ embryos. The *Shh*^{tm1amc} null allele (Dassule et al., 2000) (referred to as *Shh*$^{+/-}$) was maintained on a Swiss Webster background and crossed with *Prx*$^{Cre/+}$*;Smarcc1*$^{c/+}$ mice to generate double knockout (*Prx*$^{Cre/+}$*;Smarcc1*$^{c/c}$*;Shh*$^{-/-}$; referred to as DKO) embryos. The *Gli3*$^{Xt\text{-}J}$ (Jackson Cat# 000026; referred to as *Gli3*$^{+/-}$) allele was maintained on a Swiss-Webster background.

In situ hybridization

For colorimetric in situ hybridization embryos were treated with 10µg/mL proteinase K (Invitrogen 25530015) for 30 minutes, post-fixed, pre-hybridized at 68°C for 1hour and hybridized with 500ng/mL digoxigenin-labeled riboprobes at 68°C overnight as previously described (Lewandowski et al., 2015). BM purple (Sigma-Aldrich 11442074001) staining was visualized in dissected forelimbs using a table-top Leica light microscope equipped with a DFC420C Leica camera.

Fluorescent in situ hybridization was conducted using HCR v3.0 reagents as previously described (Ramachandran et al 2022). Briefly embryos were fixed overnight at 4°C in 4% PFA/PBS and rehydrates with MeOH/PBST (0.1% Tween-20). Embryos were then treated with 10µg/mL proteinase K for 30 minutes, incubated in 4nM probe overnight at 37°C, and then in 60pmol hairpin overnight at room temperature. After hairpin incubation, the samples were washed and counterstained in DAPI (1:5000 dilution; Life Technologies D1306), embedded in low-melt agarose and cleared in CeD3++ as described (Anderson et al., 2020). Samples were imaged on a Nikon W1 spinning disk confocal.

RNA-seq

Paired forelimbs were dissected from 2 individually genotyped control and *Prx*$^{Cre/+}$*;Smarcc1*$^{c/c}$ embryos at E11.5 (39-40 somites). RNA was extracted using Trizol reagent (Life Technologies, 15596026). Libraries were generated by BGI Genomics: samples were 3'adepylated, adaptor ligated, UDG digested, and circularized following amplification to generate a DNA nanoball that was then paired-end sequenced on a DNBSEQ platform at a depth of 40 million reads/sample. Sequenced reads were aligned to the mm10 mouse genome using Salmon (version 1.9.0) and assembled into genes using R package tximeta (version 1.16.0) (Love et al., 2020). Differential gene expression was calculated using DESeq2 (Love et al., 2014). We defined significantly differentially expressed genes using an FDR<0.05. Differentially expressed genes are listed in Source data 5.

ATAC-seq

Anterior forelimb pairs from 2 E11.5 (40-48s) control (*Prx*$^{+/+}$*;Smarcc1*$^{c/c}$)and 3 *Prx*$^{Cre/+}$*;Smarcc1*$^{c/c}$ embryos were dissected and each was used as a single biological replicate. ATAC-Seq was performed as described previously (Lex et al., 2022). Briefly limbs were dissociated in 100µg/mL Liberase (Roche 05401119001), lysed for 10minutes at 4°C in nuclear permeabilization buffer

and centrifuged for 10 minutes. Nuclei were then resuspended, and 50,000 nuclei from each replicate were incubated with 2.5µl Transposase (Illumina 20034210) in a 50µl reaction. The transposase reaction was carried out for 1hour at 37°C, shaking gently. Libraries were generated using the NEB High-Fidelity 2x Mix (New England Biolabs M0541S), PCR amplified for 11 cycles and cleaned up using SparQ PureMag beads (QuantaBio 95196-060). Libraries were sequenced using paired-end 75bp reads at a depth of ~40 million reads/sample. Samples were mapped to the mm10 mouse genome using Bowtie2 (version 2.3.5) (Trapnell et al., 2012), peaks were called using MACS2 (Zhang et al., 2008), normalized using library size parameters, and differential analysis was performed using Limma (Ritchie et al., 2015). Significantly changed peaks were called using an FDR<0.05. Differentially ATAC-accessible regions are listed in Source data 3.

Chromatin binding

For wild-type (Swiss Webster) CUT&RUN experiments, pairs of whole forelimbs at E9.25 (21-24 somites) were pooled to allow for sufficient cell numbers; for E11.5 (43-44 somites), anterior and posterior halves of forelimbs were processed individually. 2 biological replicates were collected at E9.25 and 3 biological replicates were collected at E11.5. For differential CUT&RUN , the anterior halves of forelimb pairs were collected from single, genotyped control (*Gli3*$^{+/+}$) and *Gli3*$^{-/-}$ embryos. 3 biological replicates were collected for each genotype. Dissected tissues were dissociated in 100µg/mL Liberase at 37°C for 10minutes and processed using EpiCypher's CUTANA kit reagents (EpiCypher 15-1016) and protocol with the following modifications. Following dissociation, samples were incubated overnight at 4°C with 1:50 SMARCC1 primary antibody (Invitrogen PA5-30174). Samples were then incubated with 1:100 donkey anti-rabbit (Jackson ImmunoResearch 711-035-152) secondary antibody for 30 minutes at room-temperature, washed in digitonin wash buffer and incubated with CUTANA pAG-MNase for 10minutes at RT. The Mnase reaction was then performed at 4°C for 2 hours. Libraries were generated using the NEBNext Ultra II DNA library prep kit (New England Biolabs E7645S) with 14 PCR cycles using

unique dual indexes (New England Biolabs E6440S). Following clean-up with SparQ PureMag beads (QuantaBio), samples were sequenced using PE150 at a read depth of ~5 million reads. Samples were mapped to the mm10 mouse genome using Bowtie2 (version 2.3.5) (Trapnell et al., 2012), peaks were called using MACS2 (Zhang et al., 2008). Called peaks for wild-type CUT&RUN for SMARCC1 at E11.5 and E9.25 and a list of overlapping VISTA enhancers at E11.5 are provided in Source data 1.

Differential SMARCC1 binding between E11.5 (40-43s) control (*Gli3*$^{+/+}$; n=3) and *Gli3*$^{-/-}$ (n=4) samples was conducted using an E.coli spike-in (EpiCypher 18-1401) of 0.125ng/sample. Samples were sequenced on the Novaseq platform using PE150 at a read depth of ~7 million reads. Sequenced reads were aligned to the mouse reference genome mm10 using Bowtie2 (Trapnell et al., 2012) and peaks were called using MACS2 (Zhang et al., 2008) with an FDR<0.05. For Figure 3E, enrichment values were counted from the previously published list of 309 GLI enhancers (Lex et al., 2022) and normalized using library size first, and then were Log2 transformed. For control and mutant groups respectively, the average value across biological replicates was used to calculate the final fold enrichment. All called peaks are listed in Source data 4.

Previously published H3K27ac ChIP-seq samples from E11.5 forelimbs (n=2) (GEO accession # GSE151488; (Malkmus et al., 2021)) were aligned to the mm10 mouse genome to generate ChIP-seq tracks and peak-called using Bowtie2 (Trapnell et al., 2012) and MACS2 (Zhang et al., 2008) respectively with an FDR<0.05 as cutoff. Significantly called peaks are listed in Source data 1.

Western Blot

Western blots were performed on individually genotyped E11.5 (43-48s) control (taken from a combination of *Prx*$^{+/+}$*;Smarcc1*$^{c/+}$ and *Prx*$^{+/+}$*;Smarcc1*$^{c/c}$; 4 replicates) and *Prx*$^{Cre/+}$*;Smarcc1*$^{c/c}$ (4

replicates) forelimb pairs. Approximately ~400K cells per sample were loaded onto a 4-20% gradient agarose gel (Biorad 4561094), blocked in 5% BSA for 1 hour, and then incubated with the following primary antibodies for 2 hours at room temperature in 5% BSA: 1:1000 anti-SMARCA4 (Cell Signaling Technologies 49360T) and anti-GAPDH (Cell Signaling Technologies 5174s). Samples were then incubated in secondary antibodies for 1 h at room temperature in 3% BSA: 1:5000 Donkey anti-Rabbit (Jackson 711-035-152). Blots were developed using Amersham ECL Prime (Cytiva RPN2232). Uncropped Blot images are provided in Source data 2.

Skeletal Preparation

Skeletons of Postnatal (P) day 0 mouse pups were prepared as described (Allen et al., 2011). Briefly pups were harvested, skinned, eviscerated and fixed in ethanol and acetone. Skeletons were then stained in an Alcian blue/Alizarin red stain solution for 4 days, incubated in 1% potassium hydroxide and cleared in glycerol. Skeletons were imaged using a table top Leica light microscope.

ACKNOWLEDGEMENTS

We thank Dr. Kyunghee Choi and Dr. Rho Hyun Seong for providing the *Smarcc1* mouse strain. We thank the Genomic Sequencing and Analysis Facility at UT Austin, Center for Biomedical Research Support (RRID#: SCR_021713). This work was supported by NIH R01HD073151 (to SAV and HJ) and F31DE027597 (to R.K.L.).

FIGURE LEGENDS

Figure 1. SMARCC1 binds to active limb enhancers and GLI binding regions. A. SMARCC1 binding regions in anterior and posterior halves of E11.5 wild-type forelimbs

identified by CUT&RUN (n=3). B. SMARCC1 and previously identified H3K27ac binding in E11.5 forelimbs are co-enriched. C. Most VISTA limb enhancers are bound by SMARCC1. D. Intersection of all anterior SMARCC1-binding regions with previously identified E10.5 GLI3 binding regions. E. GLI3 anterior SMARCC1 binding at select GLI target genes.

Figure 2. SMARCC1 has GLI-independent roles in regulating chromatin accessibility. A, B. Differential ATAC-seq on E11.5 control (*Prx*$^{+/+}$*;Smarcc1*$^{c/c}$; n=2) and *Prx*$^{Cre/+}$*;Smarcc1*$^{c/c}$ (n=3) anterior forelimbs. Normalized enrichment plot indicates ATAC enrichment for all regions (grey; n=100,188) and all GLI enhancers (magenta; n=309). C. ATAC fold enrichment in control vs. *Prx*$^{Cre/+}$*;Smarcc1*$^{c/c}$ samples across all ATAC accessible regions (grey) and GLI enhancers (magenta) showing significantly decreased accessibility in mutants (Wilcoxon signed rank test; ***p<2.2e-16). D. Approximately half of GLI enhancers have altered ATAC accessibility in *Prx*$^{Cre/+}$*;Smarcc1*$^{c/c}$ forelimbs. E, F. Tracks showing GLI3 binding (green), and ATAC accessibility in control and mutant samples.

Figure 3. GLI3 does not recruit or maintain SMARCC1 at enhancers. A. SMARCC1 binds to a minority of H3K27ac-enriched (H3K27ac^{+}), promoter-proximal GLI-bound enhancers (GLI-enh.) at E9.25 (21-24s). B,C. Representative tracks showing GLI3 and H3K27ac enrichment at previously defined nascent GLI enhancers with (B) and without (C) SMARCC1 binding (magenta) at E9.25. D. SMARCC1 binding determined by CUT&RUN on control (*Gli3*$^{+/+}$; n=3) and *Gli3*$^{-/-}$(n=4) anterior forelimbs at E11.5 (40-43s). E. Intersection of significant (FDR<0.05) SMARCC1 enrichment at GLI enhancers in control and *Gli3*$^{-/-}$ forelimbs. F. Fold enrichment of SMARCC1 at GLI enhancers in control and *Gli3*$^{-/-}$ forelimbs (Wilcoxon signed rank test). G,H. Representative tracks showing SMARCC1 binding at GLI enhancers.

Figure 4. *Smarcc1* is not required for GLI-repression. A. RNA-seq of E11.5 control and *Prx*$^{Cre/+}$*;Smarcc1*$^{c/c}$ forelimbs (n=2 per condition). Significantly changed genes are marked in light pink and previously predicted HH-target genes (listed in Source data 4) are highlighted in green. B. Intersection of *Gli3*-upregulated genes with either *Smarcc1*-upregulated or downregulated genes. C-J. *Sox9* expression in control (n=3; C,G), *Prx*$^{Cre/+}$*;Smarcc1*$^{c/c}$ (n=4; D,H), *Shh*$^{-/-}$ (n=4; E,I), and *Prx*$^{Cre/+}$*;Smarcc1*$^{c/c}$*; Shh*$^{-/-}$ ('DKO') (n=3; F,J) fore- (A-D) and hindlimbs (E-H) at E12.5. Scale bars denote 10mm. K-M. Proposed model showing BAF-independent GLI transcriptional repression.

REFERENCES

Allen, B. L., Song, J. Y., Izzi, L., Althaus, I. W., Kang, J.-S., Charron, F., Krauss, R. S. and McMahon, A. P. (2011). Overlapping roles and collective requirement for the coreceptors GAS1, CDO, and BOC in SHH pathway function. *Dev Cell* 20, 775–787.

Alver, B. H., Kim, K. H., Lu, P., Wang, X., Manchester, H. E., Wang, W., Haswell, J. R., Park, P. J. and Roberts, C. W. M. (2017). The SWI/SNF chromatin remodelling complex is required for maintenance of lineage specific enhancers. *Nat Commun* 8, 14648.

Anderson, M. J., Magidson, V., Kageyama, R. and Lewandoski, M. (2020). Fgf4 maintains Hes7 levels critical for normal somite segmentation clock function. *eLife* 9, e55608.

Bowers, M., Eng, L., Lao, Z., Turnbull, R. K., Bao, X., Riedel, E., Mackem, S. and Joyner, A. L. (2012). Limb anterior-posterior polarity integrates activator and repressor functions of GLI2 as well as GLI3. *Dev Biol* 370, 110–124.

Chen, J. and Archer, T. K. (2005). Regulating SWI/SNF Subunit Levels via Protein-Protein Interactions and Proteasomal Degradation: BAF155 and BAF170 Limit Expression of BAF57. *Mol Cell Biol* 25, 9016–9027.

Chen, Y., Knezevic, V., Ervin, V., Hutson, R., Ward, Y. and Mackem, S. (2004). Direct

interaction with Hoxd proteins reverses Gli3-repressor function to promote digit formation downstream of Shh. *Development* 131, 2339–2347.

Chiang, C., Litingtung, Y., Harris, M. P., Simandl, B. K., Li, Y., Beachy, P. A. and Fallon, J. F. (2001). Manifestation of the limb prepattern: limb development in the absence of sonic hedgehog function. *Dev Biol* 236, 421–435.

Clapier, C. R., Iwasa, J., Cairns, B. R. and Peterson, C. L. (2017). Mechanisms of action and regulation of ATP-dependent chromatin-remodelling complexes. *Nat Rev Mol Cell Biol* 18, 407–422.

Creyghton, M. P., Cheng, A. W., Welstead, G. G., Kooistra, T., Carey, B. W., Steine, E. J., Hanna, J., Lodato, M. A., Frampton, G. M., Sharp, P. A., et al. (2010). Histone H3K27ac separates active from poised enhancers and predicts developmental state. *Proc Natl Acad Sci USA* 107, 21931–21936.

Dai, P., Shinagawa, T., Nomura, T., Harada, J., Kaul, S. C., Wadhwa, R., Khan, M. M., Akimaru, H., Sasaki, H., Colmenares, C., et al. (2002). Ski is involved in transcriptional regulation by the repressor and full-length forms of Gli3. *Genes Dev* 16, 2843–2848.

Dassule, H. R., Lewis, P., Bei, M., Maas, R., and McMahon, A.P. (2000). Shh regulates tooth growth and morphogenesis. *Development* 127, 4775–8475.

Heintzman, N., Hon, G., Hawkins, R., Kheradpour, P., Stark, A., Harp, L., Ye, Z., Lee, L., Stuart, R., Ching, C., et al. (2009). Histone modifications at human enhancers reflect global cell-type-specific gene expression. *Nature*.

Hendy, O., Serebreni, L., Bergauer, K., Muerdter, F., Huber, L., Nemčko, F. and Stark, A. (2022). Developmental and housekeeping transcriptional programs in Drosophila require distinct chromatin remodelers. *Molecular Cell*.

Huang, B.-L., Trofka, A., Furusawa, A., Norrie, J. L., Rabinowitz, A. H., Vokes, S. A., Mark Taketo, M., Zakany, J. and Mackem, S. (2016). An interdigit signalling centre instructs coordinate phalanx-joint formation governed by 5′Hoxd–Gli3 antagonism. *Nat Commun* 7,

12903.

Jagani, Z., Mora-Blanco, E. L., Sansam, C. G., McKenna, E. S., Wilson, B., Chen, D., Klekota, J., Tamayo, P., Nguyen, P. T. L., Tolstorukov, M., et al. (2010). Loss of the tumor suppressor Snf5 leads to aberrant activation of the Hedgehog-Gli pathway. *Nat Med*.

Jeon, S. and Seong, R. H. (2016). Anteroposterior Limb Skeletal Patterning Requires the Bifunctional Action of SWI/SNF Chromatin Remodeling Complex in Hedgehog Pathway. *PLoS Genet* 12, e1005915.

Lewandowski, J. P., Du, F., Zhang, S., Powell, M. B., Falkenstein, K. N., Ji, H. and Vokes, S. A. (2015). Spatiotemporal regulation of GLI target genes in the mammalian limb bud. *Developmental Biology* 406, 92–103.

Lex, R. K., Ji, Z., Falkenstein, K. N., Zhou, W., Henry, J. L., Ji, H. and Vokes, S. A. (2020). GLI transcriptional repression regulates tissue-specific enhancer activity in response to Hedgehog signaling. *eLife* 9, e50670.

Lex, R. K., Zhou, W., Ji, Z., Falkenstein, K. N., Schuler, K. E., Windsor, K. E., Kim, J. D., Ji, H. and Vokes, S. A. (2022). GLI transcriptional repression is inert prior to Hedgehog pathway activation. *Nat Commun* 13, 808.

Litingtung, Y., Dahn, R. D., Li, Y., Fallon, J. F. and Chiang, C. (2002). Shh and Gli3 are dispensable for limb skeleton formation but regulate digit number and identity. *Nature* 418, 979–983.

Logan, M. P. O., Martin, J. F., Nagy, A., Lobe, C., Olson, E. N. and Tabin, C. J. (2002). Expression of Cre Recombinase in the developing mouse limb bud driven by a Prxl enhancer. *Genesis* 33, 77–80.

Lopez-Rios, J., Speziale, D., Robay, D., Scotti, M., Osterwalder, M., Nusspaumer, G., Galli, A., Holländer, G. A., Kmita, M. and Zeller, R. (2012). GLI3 Constrains Digit Number by Controlling Both Progenitor Proliferation and BMP-Dependent Exit to Chondrogenesis. *Dev Cell* 22, 837–848.

Love, M. I., Huber, W. and Anders, S. (2014). Moderated estimation of fold change and dispersion for RNA-seq data with DESeq2. *Genome Biology* 15, 550.

Love, M. I., Soneson, C., Hickey, P. F., Johnson, L. K., Pierce, N. T., Shepherd, L., Morgan, M. and Patro, R. (2020). Tximeta: Reference sequence checksums for provenance identification in RNA-seq. *PLOS Computational Biology* 16, e1007664.

Malkmus, J., Ramos Martins, L., Jhanwar, S., Kircher, B., Palacio, V., Sheth, R., Leal, F., Duchesne, A., Lopez-Rios, J., Peterson, K. A., et al. (2021). Spatial regulation by multiple Gremlin1 enhancers provides digit development with cis-regulatory robustness and evolutionary plasticity. *Nat Commun* 12, 5557.

Mo, R., Freer, A. M., Zinyk, D. L., Crackower, M. A., Michaud, J., Heng, H. H., Chik, K. W., Shi, X. M., Tsui, L. C., Cheng, S. H., et al. (1997). Specific and redundant functions of Gli2 and Gli3 zinc finger genes in skeletal patterning and development. *Development* 124, 113–123.

Park, Y.-K., Lee, J.-E., Yan, Z., McKernan, K., O'Haren, T., Wang, W., Peng, W. and Ge, K. (2021). Interplay of BAF and MLL4 promotes cell type-specific enhancer activation. *Nat Commun* 12, 1630.

Rada-Iglesias, A., Bajpai, R., Swigut, T., Brugmann, S. A., Flynn, R. A. and Wysocka, J. (2011). A unique chromatin signature uncovers early developmental enhancers in humans. *Nature* 470, 279–283.

Rafati, H., Parra, M., Hakre, S., Moshkin, Y., Verdin, E. and Mahmoudi, T. (2011). Repressive LTR Nucleosome Positioning by the BAF Complex Is Required for HIV Latency. *PLOS Biology* 9, e1001206.

Ritchie, M. E., Phipson, B., Wu, D., Hu, Y., Law, C. W., Shi, W. and Smyth, G. K. (2015). limma powers differential expression analyses for RNA-sequencing and microarray studies. *Nucleic Acids Res* 43, e47.

Scherz, P. J., McGlinn, E., Nissim, S. and Tabin, C. J. (2007). Extended exposure to Sonic hedgehog is required for patterning the posterior digits of the vertebrate limb. *Dev Biol* 308,

343–354.

Shi, X., Zhang, Z., Zhan, X., Cao, M., Satoh, T., Akira, S., Shpargel, K., Magnuson, T., Li, Q., Wang, R., et al. (2014). An epigenetic switch induced by Shh signalling regulates gene activation during development and medulloblastoma growth. *Nat Commun* 5, 5425.

Shi, X., Wang, Q., Gu, J., Xuan, Z. and Wu, J. I. (2016). SMARCA4/Brg1 coordinates genetic and epigenetic networks underlying Shh-type medulloblastoma development. *Oncogene* 35, 5746–5758.

Sohn, D. H., Lee, K. Y., Lee, C., Oh, J., Chung, H., Jeon, S. H. and Seong, R. H. (2007). SRG3 Interacts Directly with the Major Components of the SWI/SNF Chromatin Remodeling Complex and Protects Them from Proteasomal Degradation*. *Journal of Biological Chemistry* 282, 10614–10624.

Sokpor, G., Xie, Y., Rosenbusch, J. and Tuoc, T. (2017). Chromatin Remodeling BAF (SWI/SNF) Complexes in Neural Development and Disorders. *Frontiers in Molecular Neuroscience* 10,.

teWelscher, P., Zuniga, A., Kuijper, S., Drenth, T., Goedemans, H. J., Meijlink, F. and Zeller, R. (2002). Progression of vertebrate limb development through SHH-mediated counteraction of GLI3. *Science* 298, 827–830.

Trapnell, C., Roberts, A., Goff, L., Pertea, G., Kim, D., Kelley, D. R., Pimentel, H., Salzberg, S. L., Rinn, J. L. and Pachter, L. (2012). Differential gene and transcript expression analysis of RNA-seq experiments with TopHat and Cufflinks. *Nat Protoc* 7, 562–578.

Visel, A., Minovitsky, S., Dubchak, I. and Pennacchio, L. A. (2007). VISTA Enhancer Browser—a database of tissue-specific human enhancers. *Nucleic Acids Res* 35, D88–D92.

Vokes, S. A., Ji, H., Wong, W. H. and McMahon, A. P. (2008). A genome-scale analysis of the cis-regulatory circuitry underlying sonic hedgehog-mediated patterning of the mammalian limb. *Genes Dev* 22, 2651–2663.

Wang, X., Lee, R. S., Alver, B. H., Haswell, J. R., Wang, S., Mieczkowski, J., Drier, Y., Gillespie,

S. M., Archer, T. C., Wu, J. N., et al. (2017). SMARCB1-mediated SWI/SNF complex function is essential for enhancer regulation. *Nat Genet* 49, 289–295.

Xiong, Y., Li, W., Shang, C., Chen, R. M., Han, P., Yang, J., Stankunas, K., Wu, B., Pan, M., Zhou, B., et al. (2013). Brg1 Governs a Positive Feedback Circuit in the Hair Follicle for Tissue Regeneration and Repair. *Developmental Cell* 25, 169–181.

Zhan, X., Shi, X., Zhang, Z., Chen, Y. and Wu, J. I. (2011). Dual role of Brg chromatin remodeling factor in Sonic hedgehog signaling during neural development. *Proc Natl Acad Sci USA* 108, 12758–12763.

Zhang, Y., Liu, T., Meyer, C. A., Eeckhoute, J., Johnson, D. S., Bernstein, B. E., Nusbaum, C., Myers, R. M., Brown, M., Li, W., et al. (2008). Model-based Analysis of ChIP-Seq (MACS). *Genome Biol* 9, R137.

Zhang, Z., Feng, J., Pan, C., Lv, X., Wu, W., Zhou, Z., Liu, F., Zhang, L. and Zhao, Y. (2013). Atrophin-Rpd3 complex represses Hedgehog signaling by acting as a corepressor of CiR. *J Cell Biol* 203, 575–583.

Zhu, J., Nakamura, E., Nguyen, M.-T., Bao, X., Akiyama, H. and Mackem, S. (2008). Uncoupling Sonic hedgehog control of pattern and expansion of the developing limb bud. *Dev Cell* 14, 624–632.

Zhu, J., Patel, R., Trofka, A., Harfe, B. D. and Mackem, S. (2022). Sonic hedgehog is not a limb morphogen but acts as a trigger to specify all digits in mice. *Developmental Cell* 57, 2048-2062.e4.

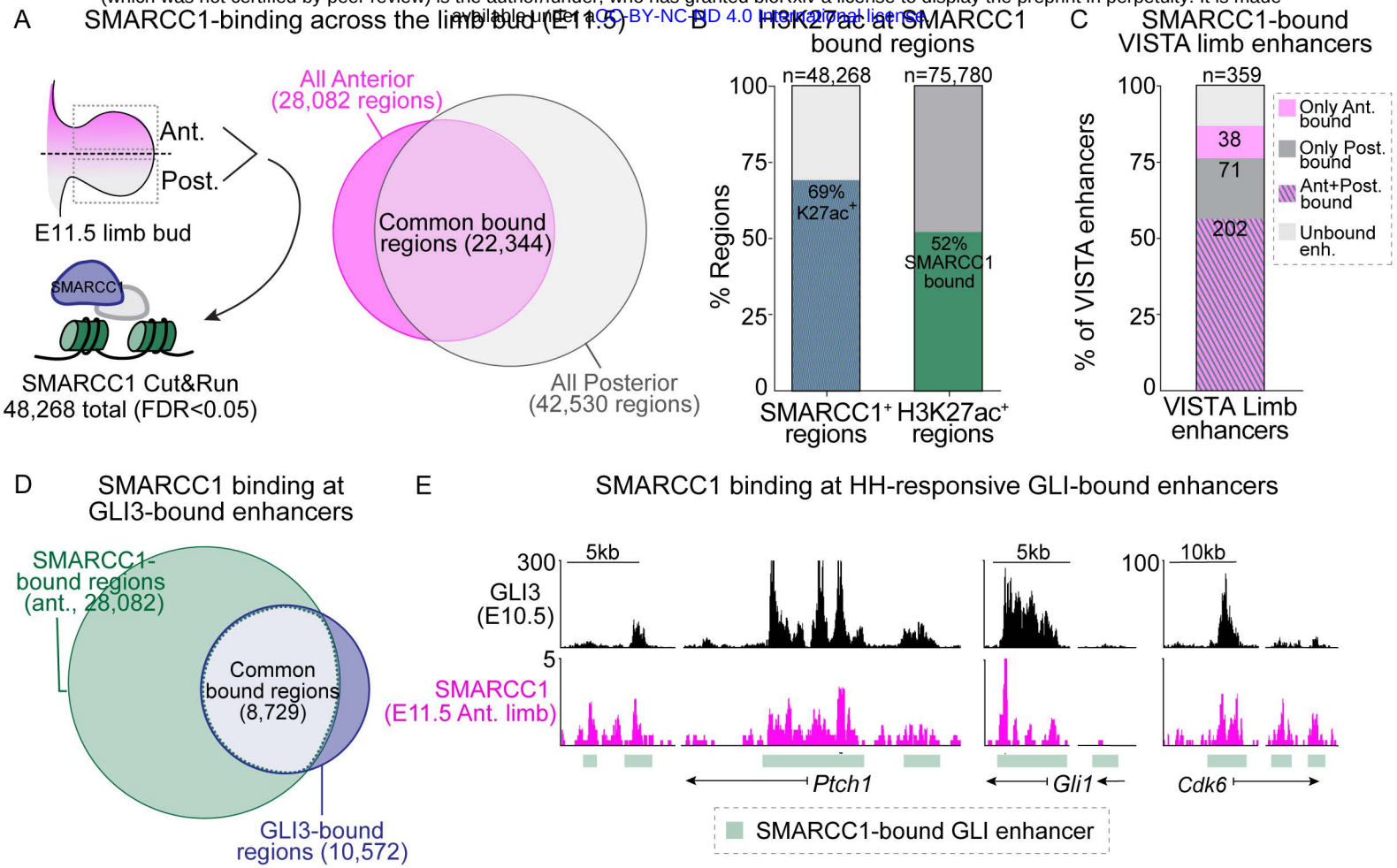

Figure 1. SMARCC1 binds to active limb enhancers and GLI binding regions.

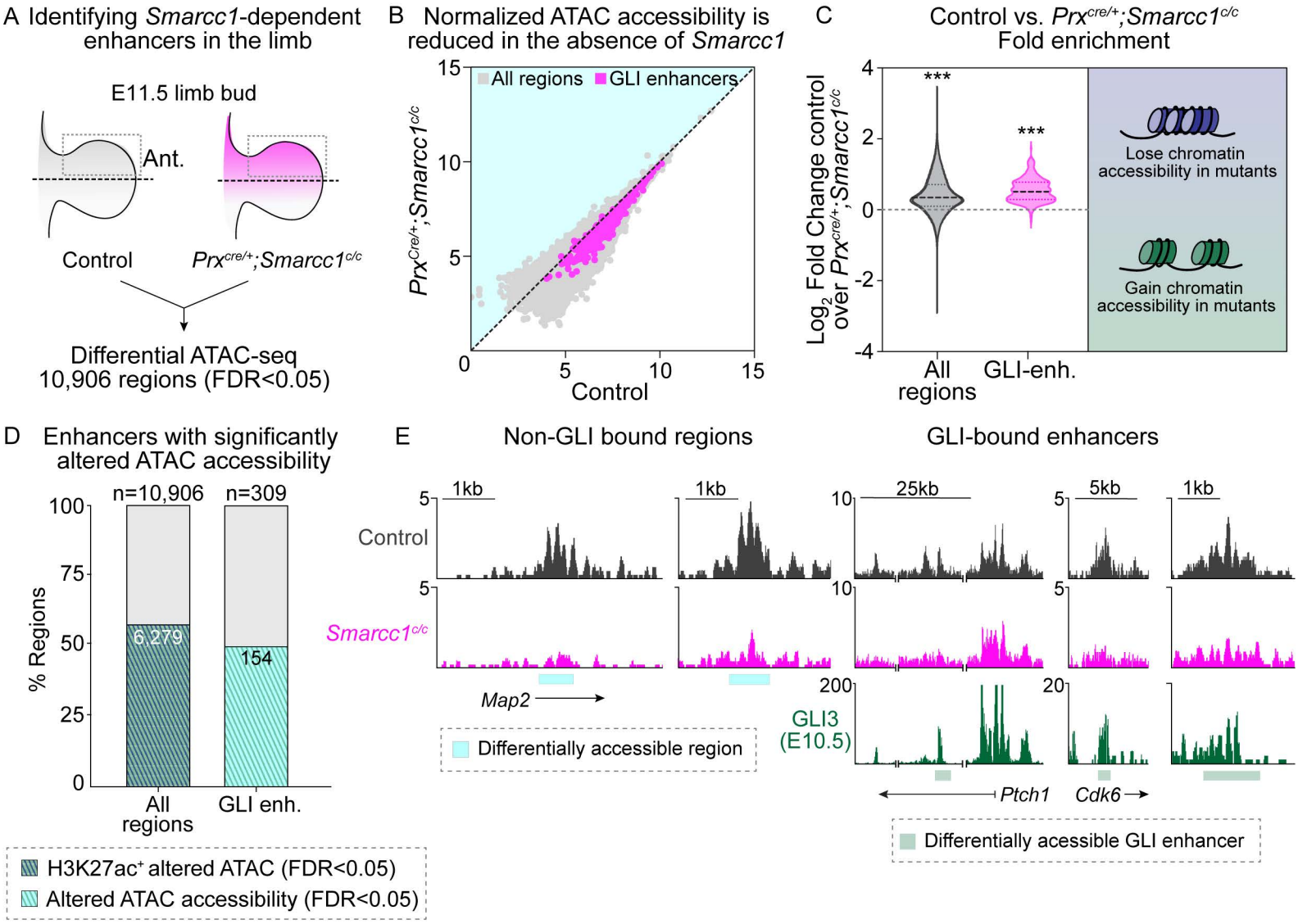

Figure 2. SMARCC1 has GLI-independent roles in regulating chromatin accessiblity.

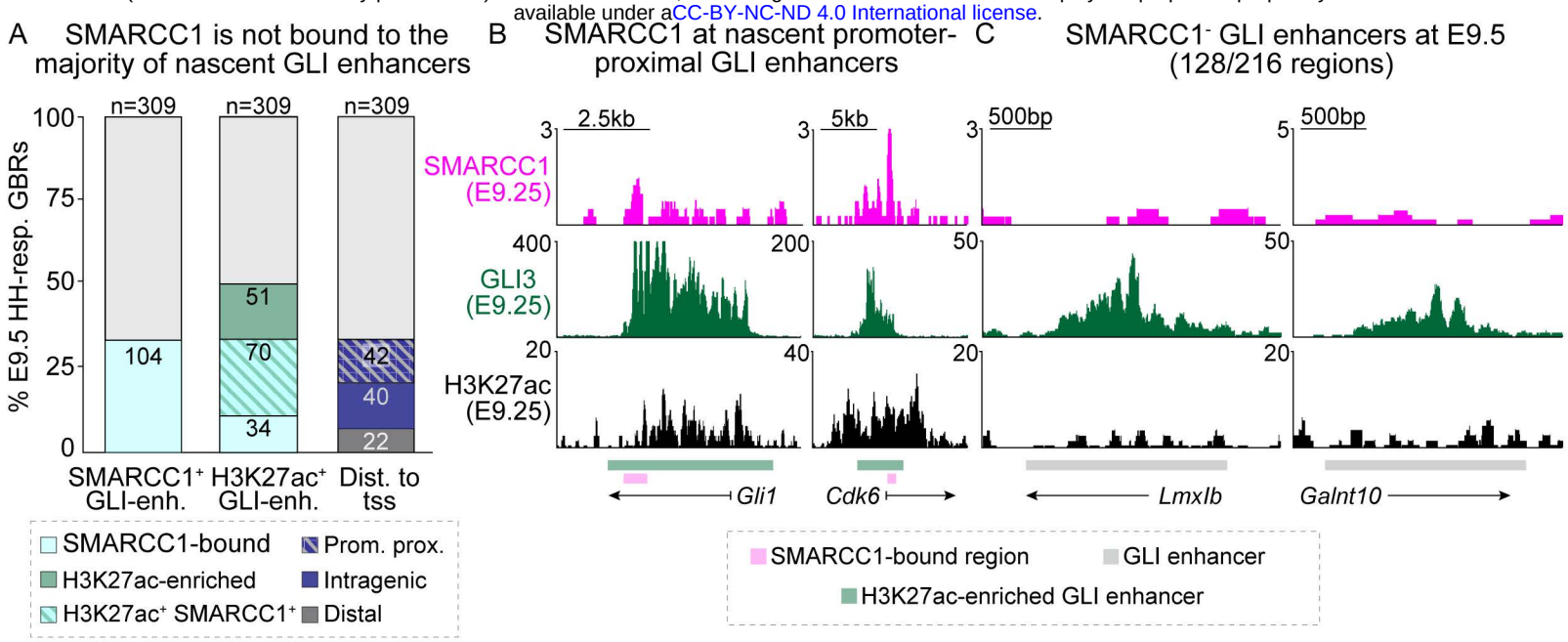

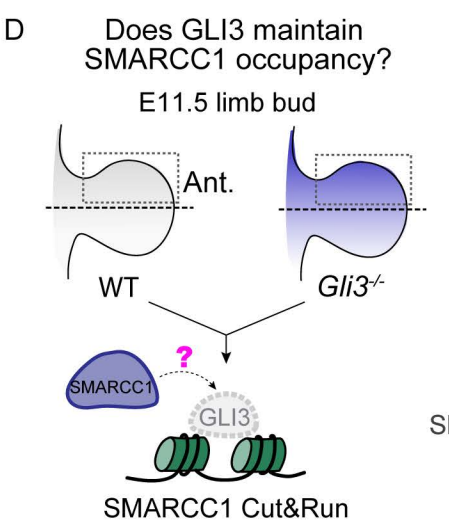

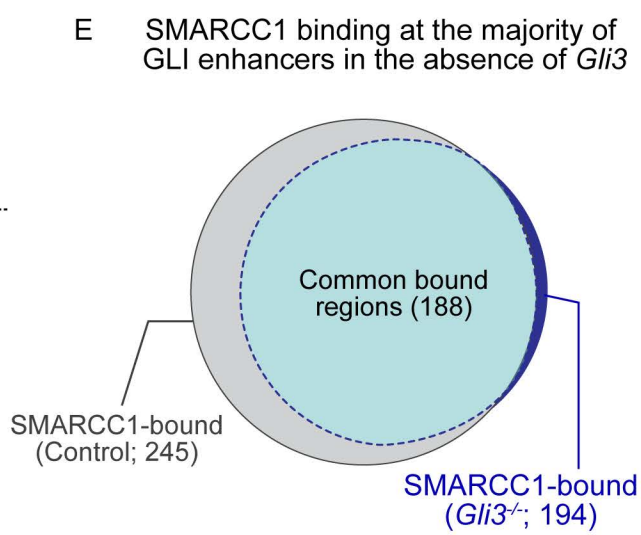

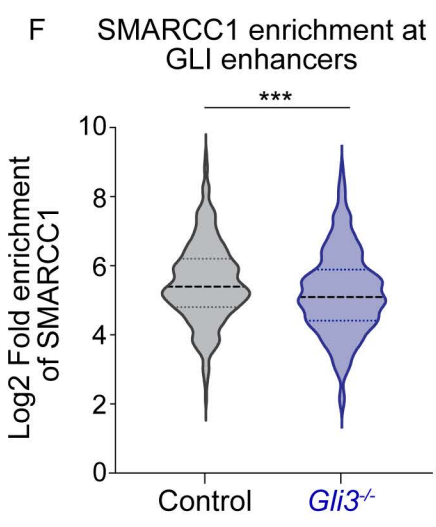

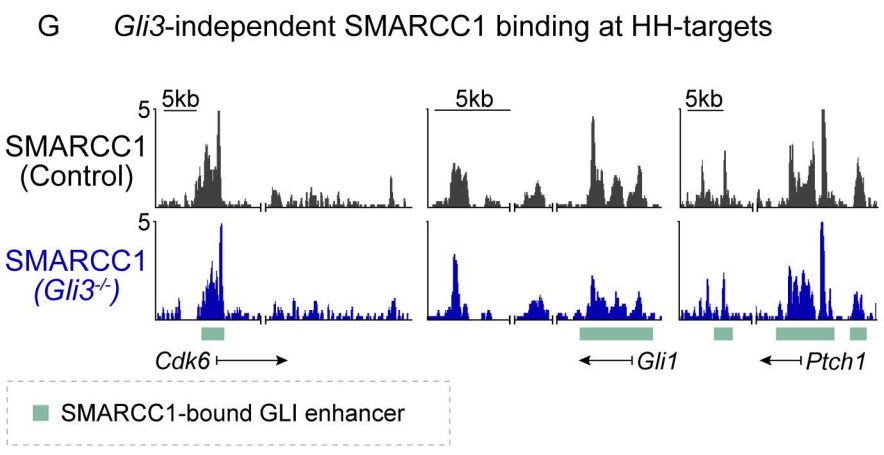

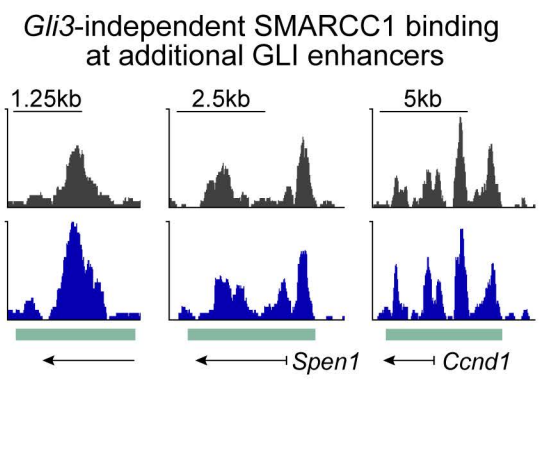

Figure 3. GLI3 does not recruit or maintain SMARCC1 at enhancers.

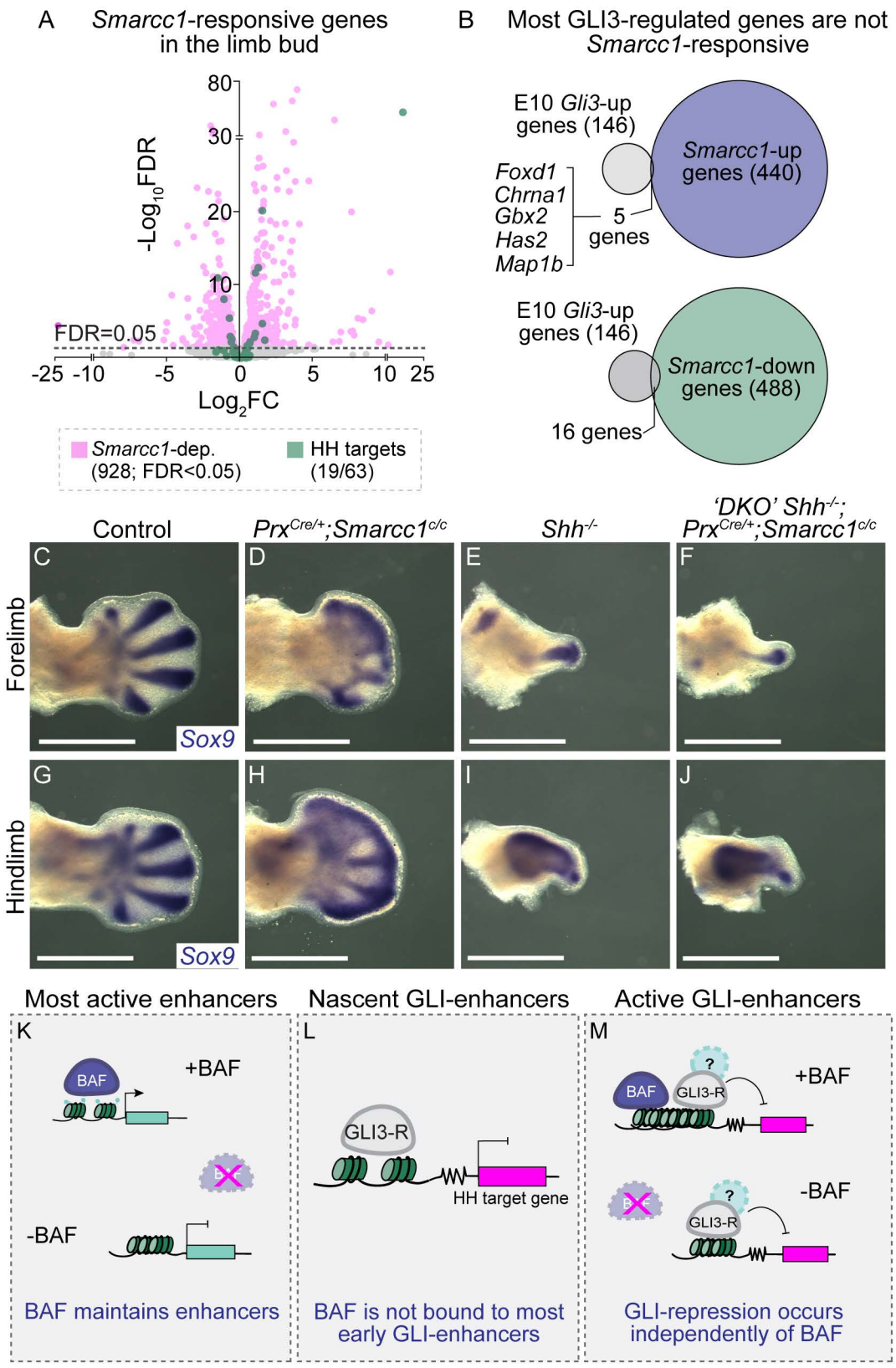

Figure 4. *Smarcc1* is not required for GLI-repression.